The Vertical Profile of Radiative Cooling and Lapse Rate in a Warming Climate

Dennis L. Hartmann , Brittany D. Dygert, Peter N. Blossey, Qiang Fu and Adam B. Sokol

Department of Atmospheric Sciences, University of Washington, Seattle, WA 98195

Corresponding author: Dennis L. Hartmann, dhartm@uw.edu

Early Online Release: This preliminary version has been accepted for publication in *Journal of the Atmospheric Sciences* cited, and has been assigned DOI 10.1175/JCLI-D-21-0861.1. The final typeset copyedited article will replace the EOR at the above DOI when it is published.

ABSTRACT: The vertical profile of clear-sky radiative cooling places important constraints on the vertical structure of convection and associated clouds. Simple theory using the cooling-to-space approximation is presented to indicate that the cooling rate in the upper troposphere should increase with surface temperature. The theory predicts how the cooling rate depends on lapse rate in an atmosphere where relative humidity remains approximately a fixed function of temperature. Radiative cooling rate is insensitive to relative humidity because of cancellation between the emission and transmission of radiation by water vapor. This theory is tested with one-dimensional radiative transfer calculations and radiative-convective equilibrium simulations. For climate simulations that produce an approximately moist adiabatic lapse rate, the radiative cooling profile becomes increasingly top-heavy with increasing surface temperature. If the temperature profile warms more slowly than a moist adiabatic profile in mid-troposphere, then the cooling rate in the upper troposphere is reduced and that in the lower troposphere is increased. This has important implications for convection, clouds and associated deep and shallow circulations.

Accepted for publication in *Journal of Climate*. DOI 10.1175/JCLI-D-21-0861.1.

1. Introduction

The global and tropical-mean atmosphere are in an approximate equilibrium where the radiative cooling of the atmosphere is balanced by the convergence of the upward flux of energy by atmospheric motions. If the clear-sky radiative cooling accounts for most of the radiative cooling of the upper troposphere, and the radiative cooling is mostly associated with water vapor, then some predictions about the dependence of convection and clouds on surface temperature can be made based on the well-understood physics of water vapor and radiative transfer. For example, Hartmann and Larson (2002) noted that the cooling from the upper troposphere is mostly from the strong lines of water vapor (Harries 1997) and that at cold temperatures the water vapor pressure becomes too low to be an effective cooling agent. This temperature occurs below the tropical tropopause and explains the observation by Folkins et al. (1999) that the transition from tropospheric to stratospheric air begins below the cold point in the Tropics. This theory also predicts that the top of the well-mixed troposphere and the cloud coverage that occurs there will remain at a nearly constant temperature as the surface warms, the so-called Fixed Anvil Temperature hypothesis.

Recent work has further explored the consequences of the line structure of water vapor and the temperature dependence of saturation vapor pressure for the radiative cooling rate of the atmosphere. Jeevanjee and Romps (2018) found for set of climate models that the radiative flux divergence in the upper troposphere is invariant with surface temperature. This implies that the cooling rate in K/day will increase with surface temperature, since particular air temperatures occur at lower pressures and densities in a warmed climate. Koll and Cronin (2018) showed that the nonlinear temperature dependencies of saturation vapor pressure and Planck emission approximately cancel to make the outgoing longwave radiation linear in surface temperature. Jeevanjee and Fueglistaler (2020b) used the line structure of water vapor and the cooling-to-space approximation to express the radiative cooling rate as a product of Planck function, a vertical emissivity gradient, and a characteristic spectral width. From this they were able to construct a simple analytic expression that predicts that at temperatures below 220K cooling by water vapor is abruptly weaker, because sufficiently strong water vapor emission lines are not available to do efficient cooling at such low vapor pressures.

Here we use the cooling-to-space approximation to explore the dependence of radiative cooling rate on temperature, relative humidity, lapse rate and pressure. This theory predicts an increase in

Accepted for publication in *Journal of Climate*. DOI 10.1175/JCLI-D-21-0861.1.

the cooling rate (K/day) in the upper troposphere with surface warming, if the relative humidity remains an approximately constant function of air temperature in a warming climate. Theory (Romps 2014a), observation (Soden et al. 2002), and model experiments (discussed later herein) suggest that relative humidity remains approximately constant as a function of temperature in the upper troposphere as the climate changes, and we will employ that approximation here. Small changes in relative humidity are expected, but their effect is normally overwhelmed by the effect of the dependence of the saturation vapor pressure on temperature. Also, our theory reveals that the effect of relative humidity on cooling rate tends to be small because of cancellation between the effects of relative humidity on emission and transmission when the vertical scale of relative humidity variations is large compared to the vertical scale of vapor pressure variations.

The theory also predicts how lapse rate will affect radiative cooling rate in these conditions. These predictions are then tested with a one-dimensional radiative transfer model. To gain a better sense of the relevance of lapse rate changes for radiative cooling we compare a global climate model result, in which the temperature profiles remain approximately moist adiabatic, with a limited domain cloud-resolving model in which the lapse rate increasingly deviates from a moist adiabat in the mid-troposphere as the climate warms. One possible explanation for the differences between the two model results is that cooling of parcels by entrainment of dry air increases the lapse rate. We employ a simple model for lapse rate variations resulting from entrainment by Zhou and Xie (2019) to illustrate how deviations from the moist adiabatic lapse rate in the mid troposphere affect the vertical structure of the cooling rate, under the assumption that relative humidity is fixed as a function of temperature.

The theory is presented in Section 2 where simple illustrations of the theory with a one-dimensional (1-D) radiative transfer model are also provided. Section 3 uses radiative-convective equilibrium (RCE) experiments with a global climate model (GCM) and a cloud-resolving model (CRM) in a small domain to show a range of model lapse rate responses to global warming. Section 4 then presents results from a 1-D RCE model to further illustrate the dependence of cooling rate on lapse rate and its response to global warming. A summary and further discussion are presented in Section 5.

Accepted for publication in *Journal of Climate*. DOI 10.1175/JCLI-D-21-0861.1.

2. Theory

a. The Cooling-To-Space Approximation

We seek a simple theoretical understanding by using the cooling-to-space (CTS) approximation (Rodgers and Walshaw 1966; Petty 2006), which is known to be an excellent approximation for the cooling from water vapor (Jeevanjee and Fueglistaler 2020a). We will use this approximation to reason how changes in temperature profile or relative humidity produce changes in cooling rate, which is dominated by the longwave emission from water vapor.

We begin with the CTS approximation for the water vapor radiative heating rate at a particular wavelength, λ (Liou (2002), p. 151).

$$\frac{dT}{dt}\Big)_\lambda = -\frac{\pi\, k_\lambda\, \rho_{H_2O}}{\rho_{Air}\, c_p\, \bar{\mu}}\, B_\lambda(T)\, e^{\frac{-\tau_\lambda}{\bar{\mu}}} \tag{1}$$

Here $\bar{\mu} = 1.66^{-1}$ is the average over a hemisphere of $\mu = cos\theta$, θ is the angle of the radiation beam from zenith, k_λ is the mass absorption coefficient, $B_\lambda(T)$ is the Planck function and τ_λ is the vertical optical depth from the given height to the top of the atmosphere. Next use the following identity

$$\frac{\rho_{H_2O}}{\rho_{Air}} = 0.622\, RH\, \frac{e_s}{p}. \tag{2}$$

Here RH represents relative humidity and e_s is the saturation vapor pressure. From the work of Chou et al. (1993) we assume a linear dependence of the mass absorption coefficient on pressure.

$$k_\lambda = k_{\lambda 0}\frac{p}{p_0} \tag{3}$$

Using (1), (2), and (3) we find that,

$$\frac{dT}{dt}\Big)_\lambda = -\frac{0.622\,\pi}{c_p\, p_0\, \bar{\mu}}\, e_s(T)\, RH\, k_{\lambda 0}\, B_\lambda(T)\, e^{\frac{-\tau_\lambda}{\bar{\mu}}}. \tag{4}$$

We write the optical depth using the hydrostatic approximation as,

Accepted for publication in *Journal of Climate*. DOI 10.1175/JCLI-D-21-0861.1.

$$\tau_\lambda = \int_z^\infty k_\lambda \, \rho_{H_2O} \, dz = \int_0^p k_{\lambda 0} \, \frac{p}{p_0} \, 0.622 \, \frac{e_s}{p} \, RH \, \rho_{Air} \, \frac{dp}{g \, \rho_{Air}}$$
$$= \frac{k_{\lambda 0} \, 0.622}{g \, p_0} \int_0^p RH \, e_s(T) \, dp \simeq \frac{k_{\lambda 0} \, 0.622}{g \, p_0} \, \overline{RH \, e_s(T)} \, p \tag{5}$$

So we can write that

$$\frac{dT}{dt}\Big)_\lambda = -\left\{ \frac{\pi \, g}{c_p} C \, k_{\lambda 0} \, B_\lambda(T) \, e_s(T) \, RH \right\} e^{\left(-C \, k_{\lambda 0} \, \overline{e_s(T) \, RH} \, p\right)}. \tag{6}$$

Where C is a constant.

$$C = \frac{0.622}{p_0 \, g \, \bar{\mu}} \tag{7}$$

The part in equation (6) in curly brackets is the emission and depends only on temperature and relative humidity, since both the saturation vapor pressure and the Planck function depend only on temperature for a fixed wavelength of radiation. The exponential part in (6) represents the transmission of this emission to space and is the only part with a pressure dependence, if we assume that the relative humidity in the upper troposhere is a function of temperature alone (see Figure 4b). The exponential part includes the mass-integrated vapor pressure above the level of emission, which varies strongly with the temperature in the layer above if the relative humidity is fixed. At a fixed temperature, the transmission (the exponential part in (6)) is likely to get larger in the upper troposphere as the surface warms because the pressure at a fixed temperature falls. In the experiments to be discussed later in this paper the pressure at the top of the layer of maximum cooling changes by nearly a factor of 2 between radiative-convective equilibrium experiments with sea-surface temperatures (SST) of 295 K and 310 K, so the exponent in the transmission part in equation (6) varies by a factor of nearly 2. This pressure dependence of the transmission causes the cooling rate in the upper troposphere to increase with surface warming.

Although (6) only applies to a single wavelength of radiation, it is known from radiative transfer theory that the maximum absorption and emission occurs where the optical depth divided by $\bar{\mu}$ is approximatly one, so that the cooling from each level is associated with absorption lines of water vapor at particular wavelengths (Harries 1997). Jeevanjee and Fueglistaler (2020b) have used this fact to show that weak lines do the cooling in the lower troposphere and strong lines do

Accepted for publication in *Journal of Climate*. DOI 10.1175/JCLI-D-21-0861.1.

the cooling in the upper troposphere, up to the point where no lines are strong enough to produce significant cooling rates at the low vapor pressures associated with the low temperatures in the upper troposphere. If one can identify the wavelengths that account for the cooling at a particular level, one can use (6) to reason how and why radiative cooling at a particular level in the atmosphere will respond to changes in temperature, pressure and relative humidity both at that level and in the overlying atmosphere.

From (5) the optical depth and the transmissivity depend on the pressure-integrated vapor pressure, or the vapor pressure path,

$$VPP = \int_0^p RH\, e_s(T)\, dp. \tag{8}$$

The cooling rate for a particular wavelength of radiation, λ, peaks where $\tau_\lambda/\bar{\mu} = 1$. Using this constraint to solve for $k_{\lambda 0}$ from (5), and substituting that result into (4), we obtain,

$$\left.\frac{dT}{dt}\right|_{\tilde{\lambda}} \approx -\left\{\frac{e^{-1}\,\pi\, g}{c_p}\, RH\; e_s(T)\; B_{\tilde{\lambda}}(T)\right\} VPP^{-1}. \tag{9}$$

Note that the absorption coefficient does not appear in (9). Here we introduce the new variable $\tilde{\lambda}$ that represents the wavelengths of radiation that have an optical depth scaled by $\bar{\mu}$ of about one at the pressure level chosen. We are assuming that one or more frequencies are passing through optical depth one at the pressure level of interest, and that most of the cooling comes from the cooling-to-space at these frequencies. These assumptions are similar to those made by Jeevanjee and Fueglistaler (2020b), who then did a simplified integral across those wavelengths. The cooling rate under these approximations is thus an emission part that depends only on the temperature and relative humidity at the level of emission, divided by the vapor pressure path above that level (VPP), which itself depends on the temperature, relative humidity and also pressure. In 9 we have chosen a pressure level and solved for the mass absorption coefficient whose corresponding optical depth is one at that pressure level. This absorption coefficient defines a range of wavelengths that must be integrated over to obtain the cooling rate . For that range of wavelengths, the cooling rate will depend inversely on the VPP above the pressure level of interest. For the rotational lines of water vapor, which do most of the cooling in the upper troposphere, wavelengths with similar

Accepted for publication in *Journal of Climate*. DOI 10.1175/JCLI-D-21-0861.1.

absorption coefficients occur near to each other, so that the wavelength dependence of the Planck function in (9) does not threaten the accuracy of our approximation.

At lower pressures the cooling rate for a particular temperature can increase because VPP becomes smaller, so that as temperatures rise to lower pressures with surface warming, we expect the cooling rate to increase. At low enough temperatures and pressures there are no absorption lines strong enough to approach an optical depth of one, and the cooling rate must decline (Hartmann and Larson 2002; Jeevanjee and Fueglistaler 2020b). If VPP becomes very large the cooling to space term becomes weak and the exchange terms that are neglected in the CTS approximation tend to cancel each other so that their contribution to cooling is also small. At high temperatures where the moist adiabatic lapse rate is small and the vapor pressure is high, the increase in VPP can reduce the ability of the lower atmosphere to cool radiatively, leading eventually a runaway greenhouse effect (Koll and Cronin 2018).

The cooling rates are less sensitive to relative humidity than to temperature for a couple of reasons. First, the vapor pressure changes by many orders of magnitude due to temperature changes with altitude via the Clausius-Clapeyron relation, while relative humidity varies by less than an order of magnitude. Second, the effects of relative humidity on emission and transmission in (6) tend to offset each other. An increase in relative humidity increases the emission in (6), but it decreases the transmission, if the vertical scale of the relative humidity variations is large compared to the e-folding depth of saturation vapor pressure. A discontinuity in relative humidity can have a significant effect, however, such as at the top of the boundary layer in subsiding regions of the Tropics.

b. Simple Illustrations of the Theory

In this section we describe some simple idealized experiments to illustrate the validity of the cooling-to-space approximation (9) and the predictions it makes about the dependence of cooling rate on vapor pressure path and relative humidity. Radiative cooling rate calculations are done with the RRTMG radiative transfer code (Iacono et al. 2000; Mlawer et al. 1997). Values of naturally occurring greenhouse gases other than water vapor are set at 350ppmv of CO_2, 1700ppbv of CH_4, 320 ppbv of N_2O and 150ppbv of CO. CFCs are set to zero. A climatological tropical profile

Accepted for publication in *Journal of Climate*. DOI 10.1175/JCLI-D-21-0861.1.

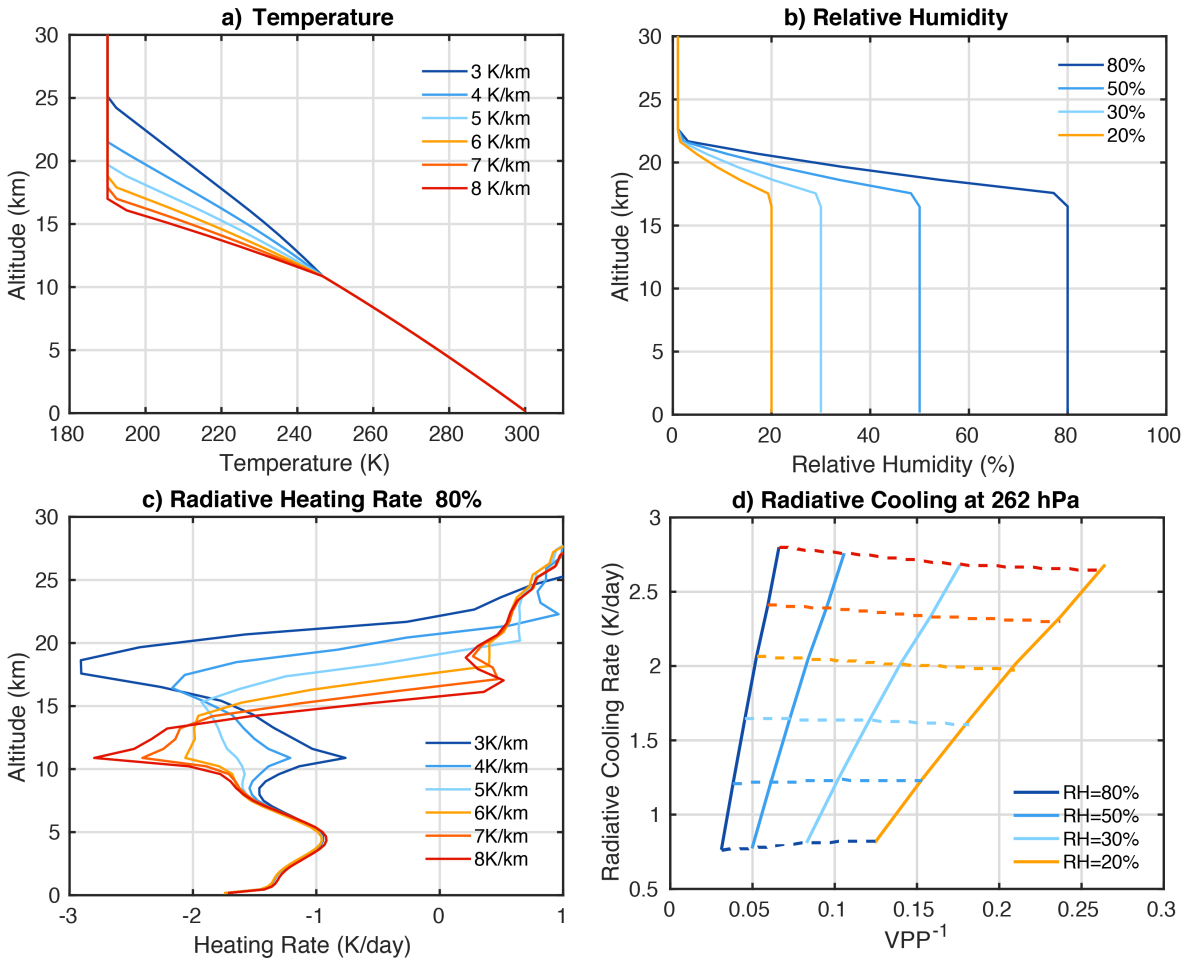

FIG. 1. a) Temperature profiles vs height, b) Relative humidity profiles vs height, c) Radiative cooling rate for the 80% relative humidity profile, but all six values of the lapse rate above 262hPa, d) Radiative cooling rate as a function of VPP^{-1} for each of the 24 cases. Solid lines follow lapse rate at fixed relative humidity, dashed lines follow relative humidity at fixed lapse rate. Dashed line colors in panel d) correspond to the temperature profiles in panel a).

of ozone is assumed. The results are not greatly affected by these assumptions, since most of the radiative absorption and emission in the troposphere is associated with water vapor.

For the first illustration we fix the lapse rate of 5 K/km as a function of log pressure using a constant scale height of 8 km and begin with a surface temperature of 300K. At 262 hPa, we change the lapse rate from 5K/km to lapse rates ranging from 3 K/km to 8 K/km. The temperature is limited to a minimum value of 190 K. These temperature profiles are shown in Figure 1a. For each of these six temperature profiles we test four relative humidity profiles that are constant below 100

Accepted for publication in *Journal of Climate*. DOI 10.1175/JCLI-D-21-0861.1.

hPa then decline to 1% above that (Figure 1b). Six temperature profiles and four relative humidity profiles give a total of 24 cases with which to study the dependence of cooling rate on lapse rate and relative humidity.

The cooling rate is shown as a function of height in Figure 1c for the 80% relative humidity profile and six values of the lapse rate above 262hPa. The cooling rate at 262hPa (≈11km) is weakest for the 3K/km lapse rate above 262hPa, because in that case the VPP above that level is largest so that the transmission term in (6) is smallest. The larger lapse rate of 8K/km above 262 hPa gives the most rapid cooling because the VPP above that level is smallest. The radiative cooling rate a few kilometers below the kink in the lapse rate is unaffected by the changing lapse rate above because the scale height of water vapor is only a few kilometers if the lapse rate is 5 K/km. The VPP at 8km is only very weakly affected by lapse rate changes above 11km. The effect of lapse rate on cooling rate changes sign at around 15km, as above this level the dominant effect shifts from the changed VPP to the changed air temperature.

Figure 1d shows the radiative cooling rate at 262 hPa versus VPP^{-1} for the 24 cases. The four solid lines in Figure 1d have six data points corresponding to the six lapse rates above 262 hPa in Figure 1a. The six dashed lines for the six lapse rates have four points corresponding to the four relative humidities in Figure 1b. The theory predicts that the cooling rate at 262 hPa will increase for greater lapse rates above 262 hPa and that for fixed relative humidity the cooling at 262 hPa will be linear in the VPP^{-1} above that level. Two things are to be noted. First, the solid lines show that the cooling rate depends linearly on VPP^{-1} as predicted by (9), indicating that the theory holds. Secondly, the dashed line show that for a fixed lapse rate the cooling rate at 262 hPa is almost independent of relative humidity. For each relative humidity the cooling rate with the 3 K/km lapse rate above 262 hPa is about 0.8 K/day, and the cooling rate with the 8 K/km lapse rate is about 2.7 K/day. The reason for this can be understood by considering (6) where the relative humidity appears both in the emission part, where higher humidity increases the cooling rate, and in the transmission part, where higher humidity decreases the cooling rate. These two effects very nearly cancel, so that the cooling rate is nearly independent of relative humidity.

We consider another illustrative case where the lapse rate is fixed at 5 K/km, but the relative humidity steps from 80% below 862 hPa to values of 80%, 50%, 30% and 20% above 862 hPa as illustrated in Figure 2a. Based on our theory, we expect the cooling rate at 862 hPa to increase

Accepted for publication in *Journal of Climate*. DOI 10.1175/JCLI-D-21-0861.1.

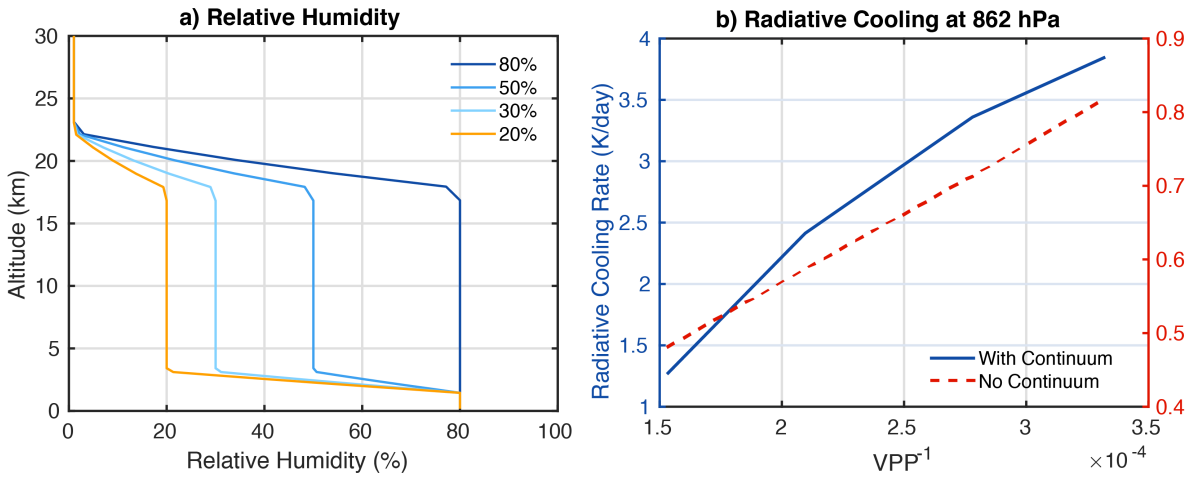

FIG. 2. a) Relative Humidity profiles vs height, b) Radiative cooling rate at 862hPa versus VPP^{-1} for the four relative humidity profiles in panel a and a uniform lapse rate of 5K/km. The dashed red line in panel b shows the radiative cooling rate without the continuum absorption of water vapor, for which the scale is on the right.

linearly with VPP^{-1} as the humidity above 862 hPa decreases. Figure 2b shows however that the cooling rate is not linear, but shows a distinct curvature. This curvature results from the importance of the continuum absorption by water vapor at high vapor pressures. Continuum absorption is not linear in vapor pressure as we assumed in the derivation of our simple theory, but rather varies as a higher power of vapor pressure (Mlawer et al. 2012). We can test that continuum absorption is the reason for the lack of linearity, and not the CTS approximation, by doing the calculation without continuum absorption. This is shown as the dashed line in Figure 2b. Without continuum absorption the radiative cooling from 862 hPa is much weaker, but it is linear in VPP^{-1} as expected from the theory. This shows that the cooling-to-space approximation holds, but our assumption of linear dependence of absorption on vapor pressure does not apply for warm temperatures where continuum absorption is very important.

From these considerations we draw three conclusions.

1) As the climate warms and upper-tropospheric temperatures move to lower pressures, the cooling rate in K/day will increase.

2) The cooling rate depends strongly on the lapse rate above the level of interest.

3) The cooling rate is insensitive to the local relative humidity, if the relative humidity varies more slowly with height than the saturation vapor pressure.

Accepted for publication in *Journal of Climate*. DOI 10.1175/JCLI-D-21-0861.1.

In addition to these expectations we have good evidence that the relative humidity in the upper troposphere will remain roughly constant as a function of air temperature during climate change (Romps 2014b). In the next section we will explore the potential impact on the cooling rate of lapse rate changes associated with global warming by contrasting a global climate model response to surface warming with that of a small-domain model.

3. GCM and CRM Comparison

To illustrate a range of lapse rate responses to global warming we compare radiative-convective equilibrium experiments with a global climate model (GCM) that uses a convective parameterization and a small-domain simulation with resolved convection (CRM). In each case four radiative-convective equilibrium simulations are performed with uniform sea surface temperatures (SST) specified to be 295, 300, 305 and 310 K. In both models there is no rotation and insolation and ozone are set to tropical values. Greenhouse gases are set to current values.

The global climate model used is GFDL's CM2.1 Global Coupled Climate Model (Anderson et al. 2004; Delworth et al. 2006). A horizontal spatial resolution of 2° latitude by 2.5° longitude, and 32 vertical levels are employed.

The CRM is the System for Atmospheric Modeling (SAM) model (Khairoutdinov and Randall 2003) with the fifth order ULTIMATE-MACHO advection scheme (Yamaguchi et al. 2011) and RRTMG radiative transfer code (Iacono et al. 2000; Mlawer et al. 1997). The Predicted Particle Properties (P3) bulk microphysics scheme is used for cloud microphysics (Morrison and Milbrandt 2015). The horizontal domain is 192x192km with 2-km resolution and periodic lateral boundary conditions. The vertical grid has 128 levels.

Figure 3 shows the net radiative cooling rate as a function of pressure and air temperature for four values of the SST in the GCM and CRM RCE simulations. Radiative cooling rates for the tropical western Pacific region based on observations are discussed by McFarlane et al. (2007). They show a profile similar to what the GCM shows for the 300K case, with cooling rates near 1.5 $Kday^{-1}$ in the upper and lower troposphere, and smaller values of about 1 $Kday^{-1}$ between the lower and upper troposphere near 700 hPa. In the GCM the cooling rate doubles in the upper troposphere as the surface is warmed from 295K to 310K, but the cooling rate in the lower troposphere is insensitive to SST (Fig. 3a). Similar increasing top-heaviness of the cooling profile is shown in

Accepted for publication in *Journal of Climate*. DOI 10.1175/JCLI-D-21-0861.1.

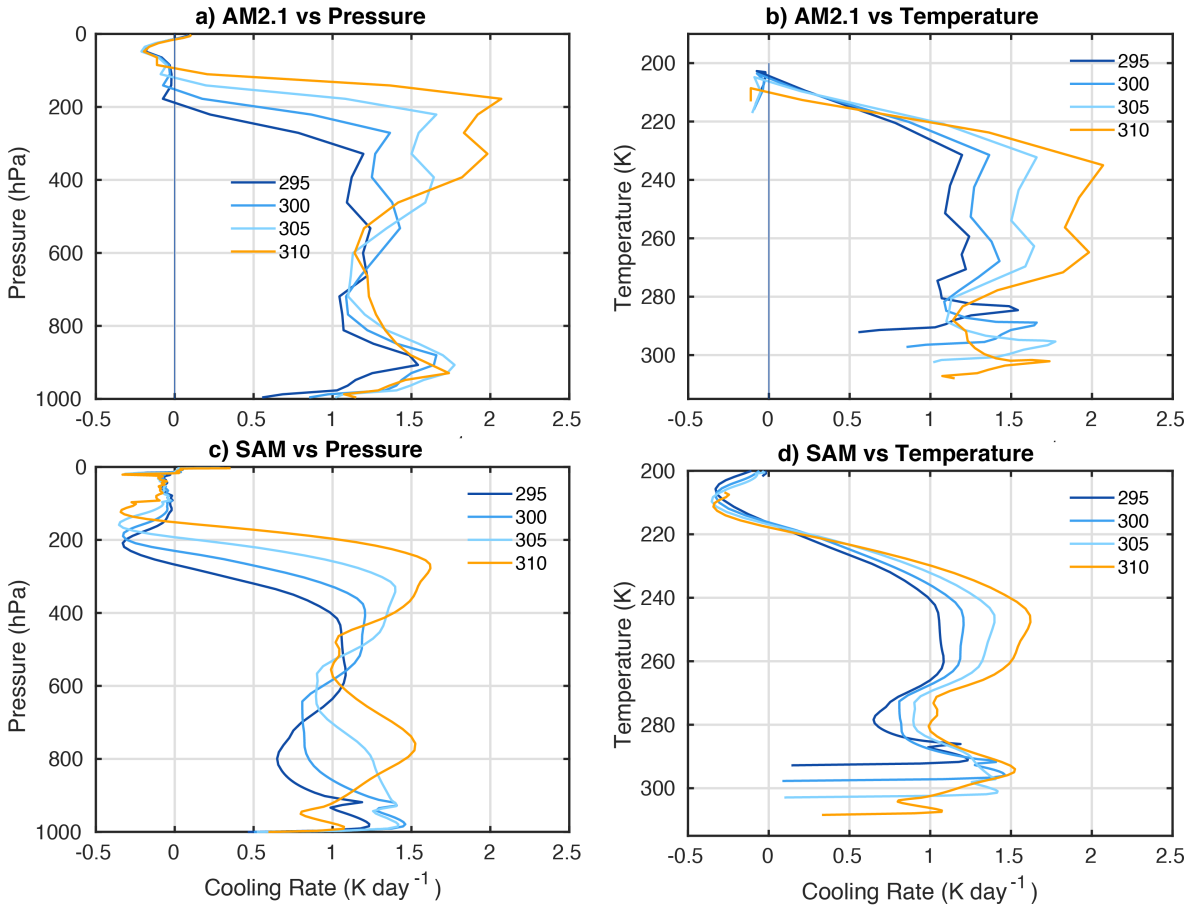

FIG. 3. Comparison of clear-sky radiative cooling rates from AM2.1 GCM as functions of pressure (a) and Temperature (b) and for the SAM CRM (c,d) in radiative-convective equilibrium with the SST values given in Kelvin.

the earlier work of Knutson and Manabe (1995), their Fig. 7. Tropospheric radiative cooling in the GCM strengthens and shifts upward to lower pressures as the sea surface temperature is raised.

In the CRM the cooling rate also increases in the upper troposphere with surface warming but at half the rate of the GCM, and the cooling rate in the lower troposphere above the boundary layer also increases, in contrast to the GCM (Figure 3c). The main cooling rate maximum in the upper troposphere occurs in a fixed temperature range because the emissivity of an atmosphere dominated by water vapor is almost entirely a function of temperature through the Clausius-Clapeyron dependence of water vapor on temperature and because of the dominance of the strong rotational emission lines of water vapor in the upper troposphere (e.g. Hartmann and Larson (2002), Jeevanjee and Fueglistaler (2020b)).

Accepted for publication in *Journal of Climate*. DOI 10.1175/JCLI-D-21-0861.1.

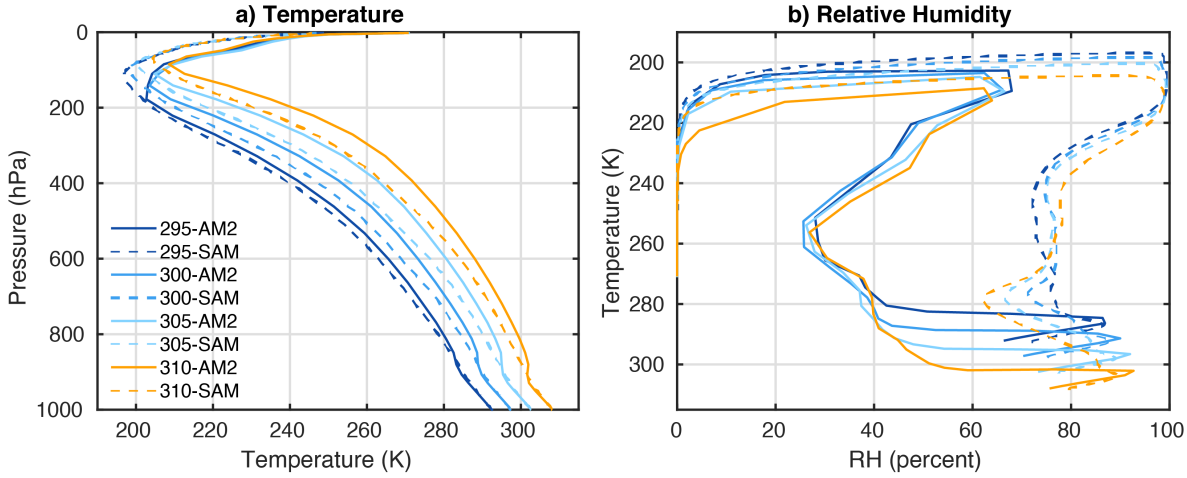

FIG. 4. Comparison of temperatures as functions of pressure (a) and relative humidities as functions of temperature (b) for the GCM and CRM simulations.

To help in understanding the differences in cooling rate we show the temperature and relative humidity profiles for the GCM and CRM in Figure 4. The GCM has temperature and humidity structures that compare well with observed tropical-mean values. These include a boundary layer inversion in the global average and a pronounced minimum in relative humidity in the mid troposphere. The GCM temperature profile follows a moist adiabat very closely above the inversion (not shown). The CRM temperature has no inversion and temperature falls off more rapidly than a moist adiabat in the lower troposphere and then more slowly to rejoin the moist adiabat in the upper troposphere. In their analysis of RCE in GCMs and CRMs Wing et al. (2020) found that large horizontal domain models were up to 10°C warmer in the mid-troposphere than small domain simulations with the same model, so much of the difference between the CRM and GCM here could be because of the domain sizes used for the simulations. Becker et al. (2018) have described how aggregation of convection can reduce updraft buoyancy reduction by shielding updrafts from mixing with dry air. Here we investigate only the possible effect of uncertainty in the lapse rate response to surface warming on the resulting radiative cooling changes.

In both models the relative humidity is a function of temperature that does not vary much above the boundary layer when the SST is changed, but the distributions are very different. An argument for why relative humidity is a function of air temperature that does not change with surface temperature has been given by Romps (2014b) based on an entraining plume model. Large-scale

Accepted for publication in *Journal of Climate*. DOI 10.1175/JCLI-D-21-0861.1.

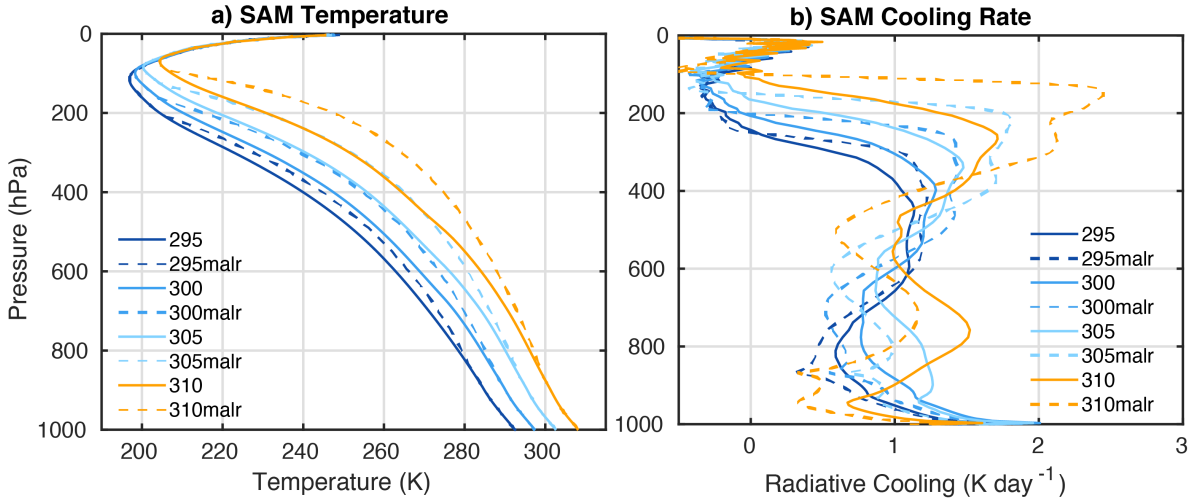

FIG. 5. a) Temperatures as a function of pressure for the CRM solution and for the solution merged to a moist adiabat at 850hPa, b) Radiative cooling rates calclated with a 1-D radiative transfer model for the temperature profiles in a). The notation malr indicates a moist adiabatic lapse rate has been assumed above 850hPa.

advection can also be employed to explain the spatial distribution of relative humidity (Soden and Bretherton 1994; Salathe and Hartmann 2000). The different relative humidity profiles are related to the convection not being aggregated in the small-domain simulations (e.g. Arnold and Putman (2018)), but here we are more interested in the lapse rate differences, since the relative humidity differences will prove to be less important for the radiative cooling rate than the lapse rate differences. In the next section we will perform some cooling rate calculations with a 1-D model to further show that the differences between the GCM and CRM cooling rates are primarily because of lapse rate difference and not differences in relative humidity.

4. One-Dimensional Model

a. Radiative Cooling Comparisons

To show the role of the temperature profile in explaining the difference in the cooling rates between the GCM and the CRM we perform offline calculations of clear-sky radiative cooling rates with a 1-D model. The 1-D model is the RRTMG radiation code described above. We perform two sets of computations, one with the relative humidity and the temperature profiles from the CRM and a second set in which the CRM temperature profile is modified to follow a moist adiabat above 850 hPa. The CRM relative humidity profile is used for both sets of simulations, with the relative

Accepted for publication in *Journal of Climate*. DOI 10.1175/JCLI-D-21-0861.1.

humidity specified as a function of temperature. These results are shown in Figure 5. Changing the temperature profile from that produced by the CRM to one that is moist adiabatic above the boundary layer causes the heating rate profile to become more top-heavy, with increased cooling rates in the upper troposphere and decreased cooling rates in the lower troposphere compared to those calculated for the CRM temperature profile.

b. Dependence of the Cooling Rate Profile on Entrainment

Zhou and Xie (2019) have noted the departures from moist adiabatic lapse rates in observations and models and proposed that entrainment of dry air can explain why the lapse rate is greater than moist adiabatic in the lower troposphere and then merges back into the moist adiabat in the upper tropical troposphere. They have proposed a 'Spectral Plume Model' (SPM) to account for the cooling of temperature profiles below the moist adiabat by entrainment of dry air. The SPM gives a more realistic temperature profile than the 'Zero Buoyancy' approximation (Singh and O'Gorman 2013), since in observations the temperature profile rejoins the moist adiabat in the upper troposphere (e.g. Folkins (2002)). The SPM gives a lapse rate that is greater than moist adiabatic in the lower troposphere and less than moist adiabatic in the upper troposphere. Our theory tells us that entrainment-modified lapse rates should result in greater radiative cooling in the lower troposphere and less radiative cooling in the upper troposphere compared to a moist adiabatic temperature profile.

Here we present 1-D radiative-convective equlibrium (RCE) calculations where we use the SPM of Zhou and Xie (2019) to enforce deviations from the moist adiabatic lapse rate. The surface temperature is fixed and the lapse rate is adjusted to the lapse rate obtained from the SPM with a range of entrainment parameters. We use exactly the same SPM formulation as Zhou and Xie (2019), except that we fix the base of the entrainment layer at about 850hPa and we set the top of the entrainment layer where the radiative cooling rate is smaller than 0.4 $Kday^{-1}$, which defines the top of the convecting layer. Energy is conserved while enforcing an upper limit on the lapse rate using a convective adjustment similar to Manabe and Wetherald (1967). In the results shown here the entrainment parameter is varied from $\epsilon_0 = 0.0\ km^{-1}$ to $0.5\ km^{-1}$, with the larger values of 0.4 and $0.5\ km^{-1}$ providing a reasonable fit to the SAM CRM over the range of SST we consider. Bao et al. (2021) also studied the effect of deviations from the moist adiabat using a similar plume

Accepted for publication in *Journal of Climate*. DOI 10.1175/JCLI-D-21-0861.1.

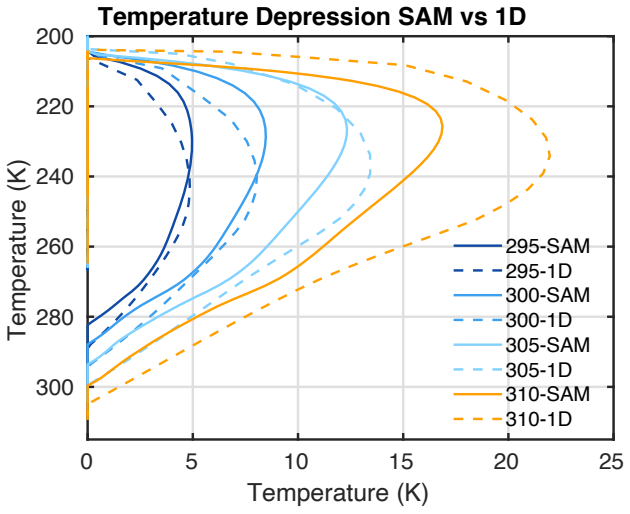

FIG. 6. Depression of the temperature profile from a moist adiabat starting at 850hPa for the CRM simulations and the 1-D model with an entrainment parameter of 0.5 km^{-1} with an assumption of 80% relative humidity over liquid and ice in the troposphere.

model in one-dimensional models and found that the deviations associated with larger entrainment led to larger estimated climate sensitivity. Here we focus more on the vertical structure of the radiative cooling.

The relative humidity can be specified as a dynamic function of pressure, temperature and cooling rate. To provide a simple case for interpretation, we assume that the relative humidity is a constant 80% in the troposphere, up to the top of the convecting layer where the cooling rate falls below 0.4 $Kday^{-1}$. The top of the convecting layer and its higher humidity are thus allowed to move to lower pressure with surface warming in a somewhat natural way. The SPM, the moist adiabatic lapse rate and the radiative transfer model are all weakly dependent on the assumption of how the saturation vapor pressure transitions from that of liquid to that of ice. To further simplify the interpretation of these computations, we first assume that the saturation vapor pressure is that over liquid everywhere. The impact of this assumption can be judged by considering an alternative formulation in which the saturation vapor pressure transitions from that of vapor to that of ice between 273 K to 253 K. These differences are significant but do not affect our basic conclusions. The reduction in saturation vapor pressure between water and ice causes an additional vertical gradient in vapor pressure that creates corresponding anomalies in the heating rate consistent with the cooling-to-space theory (not shown).

Accepted for publication in *Journal of Climate*. DOI 10.1175/JCLI-D-21-0861.1.

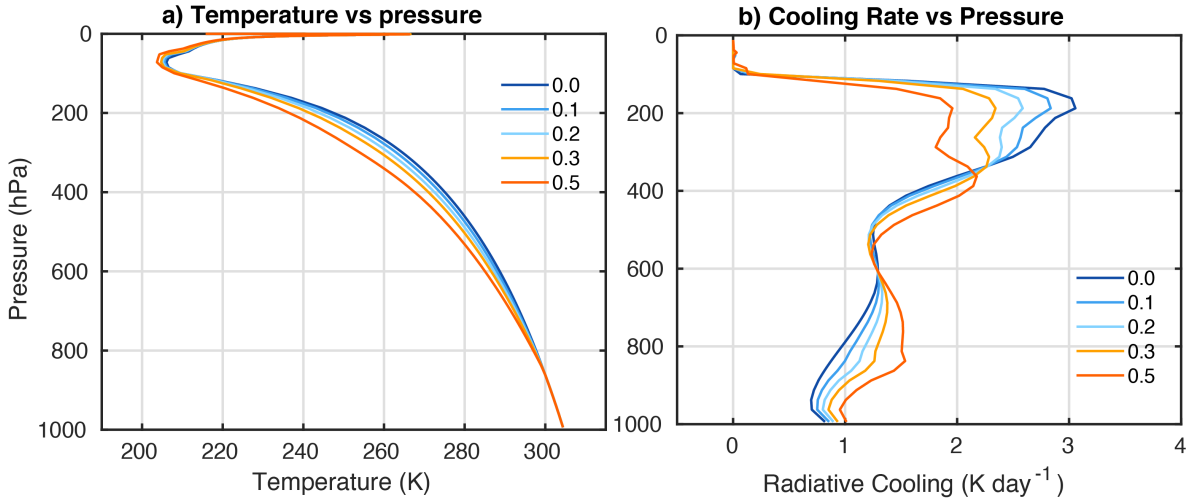

FIG. 7. One dimensional RCE model results for a surface temperature of 305K and a constant relative humidity of 80% over liquid for entrainment parameters from 0. to 0.5 km^{-1}. a) Temperatures as a function of pressure, b) radiative cooling rates as a function of pressure.

The temperature deviations from a moist adiabat in the CRM simulation and in the 1-D RCE model with an entrainment parameter of 0.5 km^{-1} are shown in Figure 6 as functions of air temperature. The spectral plume model does a reasonable job of simulating the deviation from a moist adiabat that is produced by the CRM simulation, as has been shown by Zhou and Xie (2019). A single entrainment parameter does not match the CRM results well across all SST values, and the temperature depression for the 310K case is overestimated by the spectral plume model with an entrainment parameter of 0.5 km^{-1}. The 310K case is better fit with an entrainment parameter of 0.4 km^{-1} (not shown), but that value leads to a worse fit for the lowest SST values. One could select the entrainment parameter that gives the best fit to the SAM CRM for a given surface temperature, but that would not affect our conclusions.

Figure 7 shows the temperature profiles and radiative cooling rates for the 1-D RCE model with a surface temperature of 305K and different values of the entrainment parameter in the spectral plume model of Zhou and Xie (2019). As the entrainment parameter is increased the lapse rate increases in the lower troposphere and decreases in the upper troposphere. The cooling rate increases in the lower troposphere, shows little change in the middle troposphere and weakens in the upper troposphere as the entrainment parameter is increased (Figure 7b), as one would expect from the discussion in Section 2. The cooling rate profile is most top-heavy for a moist adiabatic temperature

Accepted for publication in *Journal of Climate*. DOI 10.1175/JCLI-D-21-0861.1.

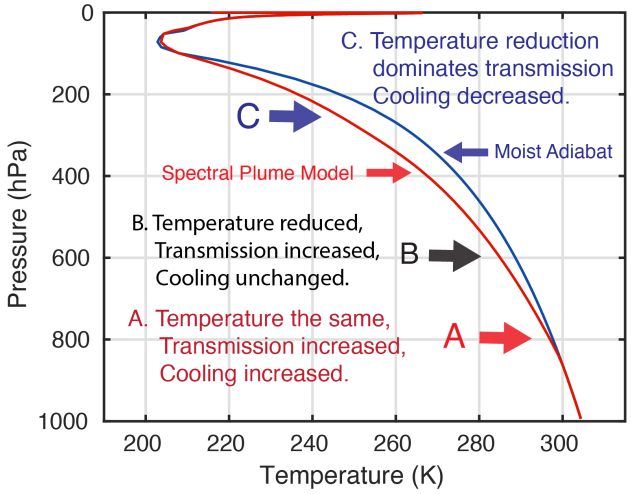

FIG. 8. One dimensional model results for a surface temperature of 305K and with entrainment parameters of 0 (blue line) and 0.5 km^{-1} (red line) as in Figure 7. Point A indicates the lower troposphere where the cooling rate increases as the entrainment parameter is increased, point B indicates the middle troposphere where the cooling rate remains unchanged, and point C indicates the upper troposphere where the cooling rate declines with entrainment parameter. The annotations describe how the cooling-to-space explains the changed cooling rates associated with departures from the moist adiabat at these levels.

profile, and the vertical gradient of the heating rate weakens with increasing entrainment. The effect of entrainment on the vertical structure of radiative cooling would be important for convection, clouds and the circulations that balance radiative cooling. In particular, strong entrainment would favor strong shallow circulations, as strong lower tropospheric radiative cooling in subsiding regions would be balanced by strong convective heating in the lower troposphere elsewhere in the domain, giving a strong shallow circulation.

c. Cooling-To-Space Interpretation of Cooling Rate Changes

A schematic diagram that describes the differences in cooling rate to be expected in going from the moist adiabatic lapse rate to the entrainment-modified lapse rate is shown in Figure 8. A fixed pressure coordinate system is used in the figure to coordinate with Figures 7a and b, and the discussion will be first phrased in a pressure coordinate system. In the lower troposphere at point A, as the entrainment parameter is increased the temperature does not change very much at that level, but the layer of air above it becomes cooler and therefore drier. So the emission part in (6)

Accepted for publication in *Journal of Climate*. DOI 10.1175/JCLI-D-21-0861.1.

does not change, but the transmission part becomes larger, since the total moisture above that level declines with increasing lapse rate. The cooling rate therefore increases in the lower troposphere, since the emission is unchanged, but the transmission to space is easier.

As one moves upward from point A to point B the temperature at a fixed pressure decreases, but because the layer above is also colder the water vapor in the layer above declines. The lowered temperature at the emission level reduces the emission, but the lowered humidity above that level increases the transmission to space so that the emission and transmission effects cancel and the cooling rate remains unchanged. This explains the crossover in mid-troposphere where the cooling rate is not affected by the departure from the moist adiabat (Figure 7b). At point C near 250 hPa the atmosphere emission is reduced because the atmosphere is cooler, but the transmission is not reduced as much in the layer above, since the lapse rate is decreased, so the cooling rate declines in response to the departure from a moist adiabatic profile.

One can also make these arguments in a reference frame of air temperature in which only the transmission part varies if the relative humidity is fixed. This is the more natural reference frame to use, since cooling rates tend to be a function of temperature through the strong control of water vapor. To aid in this interpretation we can consider the integral of vapor pressure over air pressure that appears in the equation for the optical depth (5). This integral represents the effect of the vapor pressure path above the level of interest, but takes into account the effect of pressure broadening, which the water vapor path does not. We integrate from the top of the atmosphere to a temperature T in the lower troposphere where the pressure is $p(T)$ to compute the vapor pressure path (VPP') above a particular temperature, T.

$$VPP' = \int_0^{p(T)} RH\, e_s(T)\, dp \tag{10}$$

We can linearize about the moist adiabatic temperature profile, T_{malr}, and add the effect of the temperature anomaly associated with entrainment, T'. Using the Clausius-Clapeyron relationship we obtain the following expression.

$$VPP' \approx \int_0^{p(T)} RH\; e_s(T_{malr})\left(1 + \frac{L}{R_v\, T_{malr}^2}\, T'\right) dp \tag{11}$$

Accepted for publication in *Journal of Climate*. DOI 10.1175/JCLI-D-21-0861.1.

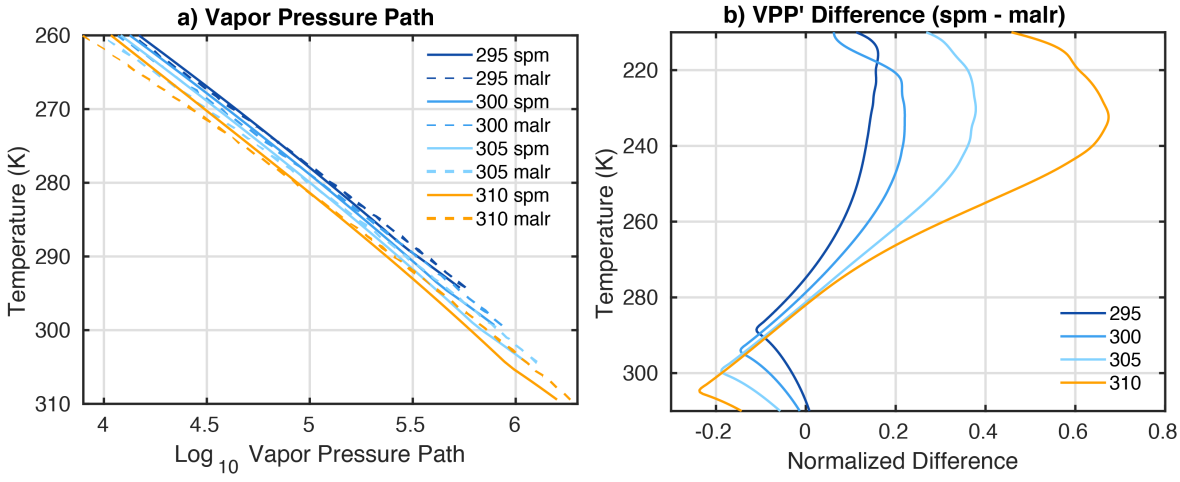

FIG. 9. a) log_{10} of VPP' from (10) for the moist adiabatic (malr) and Spectral Plume Model (spm) with an entrainment parameter of 0.5 km^{-1} with an assumption of 80% relative humidity over liquid and ice in the troposphere. b) difference between VPP' with and without entrainment at each temperature, normalized by the mean of the two values at each temperature.

A negative T' will cause the part within parentheses in (11) to be smaller and decrease the water vapor path above. On the other hand, the limit on the integral, $p(T)$ will become larger if the layer above is cooler, as can be seen in Figure 8. The effect of the cooling of the layer above and the increasing pressure of fixed temperatures can offset each other in the lower troposphere. Figure 9a shows the values of VPP' in the lower troposphere from the 1-D model for entrainment parameters of zero (moist adiabatic lapse rate) and 0.5 km^{-1}. The VPP' increases by about a factor of 10 for every 20K of temperature increase, so VPP' has little dependence on vapor more than a few kilometers above the level of interest. One can also see that at the warmest temperatures in the lower troposphere the VPP' value is less with entrainment, but is greater with entrainment at temperatures colder than about 280K.

The variation of the sign of the difference of VPP' with temperature is shown more clearly in Figure 9b, which shows the normalized difference between the cases with and without entrainment-modified lapse rates. In the warmest, lowest part of the troposphere the VPP' decreases with entrainment. Near 295 K the pressure is unchanged between the moist adiabat and the entrainment-modifed temperature profile (Figure 8), but the amount of water vapor above it is decreased because the lapse rate of temperature is greater with entrainment, so VPP' decreases and the cooling rate

Accepted for publication in *Journal of Climate*. DOI 10.1175/JCLI-D-21-0861.1.

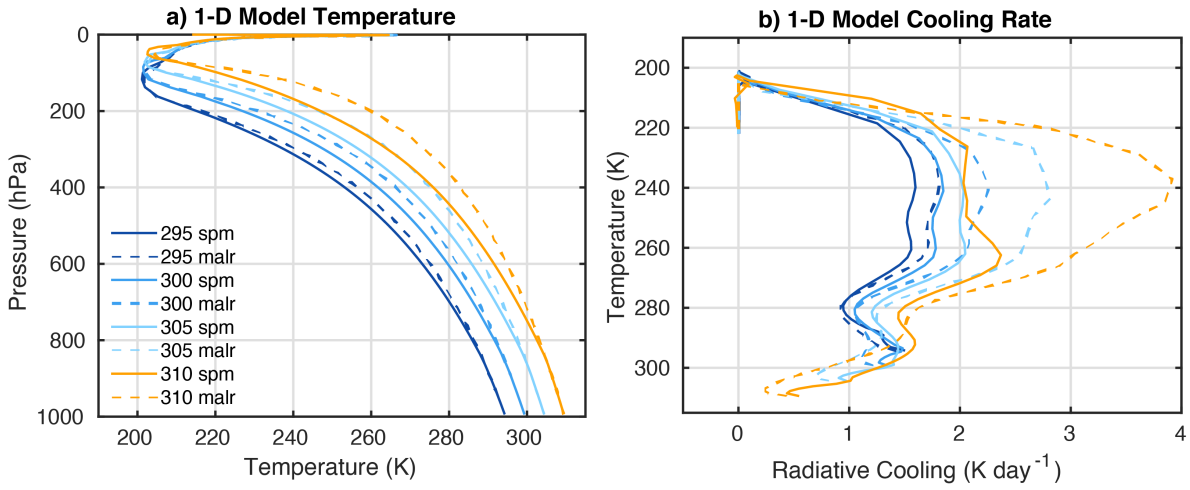

FIG. 10. One-dimensional model results for warming experiments comparing a moist adiabatic temperature profile with a temperature profile that is modified using the spectral plume model with an entrainment parameter of 0.4 km^{-1}. Dashed lines indicate the moist adiabatic profiles and solid lines the entrainment-modifed temperature profiles. a) Temperature versus pressure and b) radiative cooling rate versus air temperature.

increases. Near 280 K, the pressure is increased which would decrease transmission, but the lapse rate above is greater, so that the pressure and humidity effects on transmission can cancel exactly near 280K. Near 240 K the pressure at a fixed temperature is increased by entrainment, reducing the transmission, but the lapse rate above is less than in the moist adiabatic case so that vapor changes cannot offset pressure effects. Also the fractional change of pressure is greater in the upper troposphere, so it is harder for humidity changes to offset pressure changes. Thus the increased lapse rate of the entrainment-modified temperature profile causes the same temperature to occur at a higher pressure in the upper troposphere, so that at a fixed temperature the transmission is smaller and reduces the cooling rate. These differences explain the change in response of cooling rate to deviations from the moist adiabat as a function of temperature. Entrainment-modified lapse rates produce more cooling in the lowest troposphere, no change around 280 K and less cooling in the upper troposphere at temperatures colder than about 280K. Using the change in the temperature profile and an assumption of fixed relative humidity, one can thus reason out why the cooling rate profile responds to entrainment modifications by increasing in the lower troposphere, decreasing in the upper troposphere, and changing very little in the middle troposphere.

Accepted for publication in *Journal of Climate*. DOI 10.1175/JCLI-D-21-0861.1.

d. Cooling Rate Response to Surface Warming

In this section we use the SPM as a theory for why the temperature falls below the moist adiabat in mid-troposphere and explore the implications of that for surface warming experiments in a 1-D model. Figure 10 shows results of radiative-convective equilibrium above fixed SST for both the moist adiabatic and spectral plume model profiles for a fixed relative humidity of 80% within the convecting layer. The saturation specific humidity is determined by a linear interpolation from liquid to ice between 273 K and 253 K. The entrainment parameter is 0.4 km^{-1}, since that best fits the CRM result for the warmest temperature of 310K. For the moist adiabatic profile, the cooling rate becomes much stronger near 240 K as the surface temperature is increased. This is because the maximum cooling level near 240 K moves to a lower pressure as the surface warms, meaning that the transmission to space is easier and the cooling rate increases by more than a factor of 2. In the lowest part of the troposphere the cooling rate decreases for the warmest surface temperatures. The decreased cooling rate near the surface is because the strong absorption, especially the continuum absorption by water vapor, increases the optical depth of the lower atmosphere and makes it difficult for the lowest troposphere to cool to space. This reduction in lower tropospheric cooling marks the beginning of a process that leads to a runaway greenhouse effect. The near-surface cooling rate decrease with surface warming is reduced but still present for the entrainment-modified temperature profile. Around atmospheric temperatures of 280K the cooling rate is less sensitive to both surface temperature and to the effects of entrainment, for reasons that were outlined in Figures 8 and 9 and related discussion.

In the upper troposphere, the increase in radiative cooling with surface temperature is greatly reduced by the lapse rate changes associated with the SPM. If we consider changes at the level of strongest radiative cooling around 240 K associated with surface warming, the pressure at this temperature decreases more strongly with warming when using a moist adiabat than with the SPM temperature profile. This causes an increasing gap between between $p_{MALR}(T)$ and $p_{SPM}(T)$ with surface warming that impacts the overlying vapor pressure path, as seen in Figure 9b. As the relative difference in transmissivity increases with surface warming, so too does the radiative cooling (Figure 10b). These changes are similar in structure but larger in magnitude than the changes shown in Figure 5b for the CRM.

Accepted for publication in *Journal of Climate*. DOI 10.1175/JCLI-D-21-0861.1.

5. Summary and Conclusion

We have examined a simple theory for explaining the effect of lapse rate on radiative cooling rate in an atmosphere with relative humidity fixed as a function of temperature. If the temperature profile is nearly moist-adiabatic, the vertical structure of radiative cooling becomes more top-heavy with surface warming, as is seen in global climate models. The increasing top-heaviness of cooling is explained by the fact that the temperatures from which the cooling emerges move to lower pressures with surface warming, which eases the transmission of the emitted radiation to space and enhances the cooling rate from a fixed emission temperature. The cooling-to-space approximation can also be used to explain the response of the vertical structure of the atmospheric radiative cooling rate to atmospheric lapse rate changes. Actual lapse rates may be greater than moist adiabatic in the lower troposphere and less than moist adiabatic in the upper troposphere. The decreased temperatures in the mid troposphere, when coupled with an assumption of fixed relative humidity, cause the cooling rate to increase in the lower troposphere and decrease in the upper troposphere relative to those of a moist adiabatic temperature profile. The departures of the temperature profile from moist adiabatic may increase with global warming, which would mean that the cooling rate remains more uniform with altitude as the surface warms, rather than becoming more top-heavy as would be the case if the temperature profile remained always approximately moist adiabatic.

We also find that the sensitivity of cooling rate to relative humidity is weak. The effects of relative humidity on emission and transmission of radiation tend to cancel so that a wide range of relative humidities give nearly the same cooling rate, so long as the relative humidity varies slowly with altitude compared to the saturation vapor pressure.

The structure of radiative cooling and its response to global warming are very important for convection, clouds and atmospheric circulation. Enhanced upper-tropospheric radiative cooling implies enhanced convective heating, which may alter the ice clouds whose cloud radiative effects are very important in the tropics. The effects of more top-heavy radiative cooling rates on ice cloud properties as climate warms are investigated by Sokol and Hartmann (2022) using SAM CRM simulations similar to those described here. Enhanced cooling in the lower troposphere can support enhanced shallow circulations as well as shallow and mid-level convection and clouds, which have different climate impacts than deep convection and high clouds.

Accepted for publication in *Journal of Climate*. DOI 10.1175/JCLI-D-21-0861.1.

An important remaining question is to what extent atmospheric temperature profiles will deviate from moist adiabats in a warmed climate. Small domain CRM experiments suggest that mid-tropospheric temperatures will increasingly deviate from the moist adiabat as the climate warms. Enhanced radiative cooling in the lower troposphere in these models has important implications for the circulations that develop within the models and may help to explain why limited area RCE simulations have such a wide variety of circulations with shallow, deep and sometimes multiple mid-level circulations cells (Wing et al. 2020). Entrainment can cool the middle troposphere in the vicinity of convection, but active convection occupies a small fraction of the tropical atmosphere. Large-scale effects may act to reduce the impact of entrainment cooling in the mid troposphere implied by small-domain CRM simulations. Wing et al. (2020) have shown that mid-tropospheric temperatures are warmer in RCE simulations with larger horizontal domains. Sensitivity to domain size may result from the effect of convective aggregation on buoyancy reduction by entrainment (Becker et al. 2018). Further experimentation with high-resolution models in larger domains or experiments with global models in which parameterisations of entrainment cooling are modified may help to better understand how tropical lapse rates will respond to global warming. Since lapse rate interacts strongly with radiative cooling, as shown here, it is important to refine our understanding of what determines the equilibrium lapse rate during climate change.

Accepted for publication in *Journal of Climate*. DOI 10.1175/JCLI-D-21-0861.1.

Acknowledgments. This work was supported by the National Science Foundation under Grant AGS-1549579. QF is partially supported by NSF AGS-1821437. ABS is partially supported by NASA FINESST grant 80NSSC20K1613. PB was supported in part by NSF grant OISE-1743753. We are grateful to GFDL-NOAA for providing the GCM model code and Marat Khairoutdinov for the SAM code used here. Eli Mlawer helped with instructions for easily removing the continuum absorption from the RRTMG model code.

Data Availability Statement

All models used in this investigation are publicly available. Data for key figures and associated software are here http://hdl.handle.net/1773/47856.

References

Anderson, J. L., and Coauthors, 2004: The new GFDL global atmosphere and land model AM2-LM2: Evaluation with prescribed SST simulations. *J. Climate*, **17 (24)**, 4641–4673.

Arnold, N. P., and W. M. Putman, 2018: Nonrotating convective self-aggregation in a limited area agcm. *J. Adv. Model. Earth Sys.*, **10 (4)**, 1029–1046, https://doi.org/10.1002/2017ms001218.

Bao, J., B. Stevens, L. Kluft, and D. Jiménez-de-la Cuesta, 2021: Changes in the tropical lapse rate due to entrainment and their impact on climate sensitivity. *Geophys. Res. Lett.*, **48 (18)**, e2021GL094 969, https://doi.org/10.1029/2021GL094969.

Becker, T., C. S. Bretherton, C. Hohenegger, and B. Stevens, 2018: Estimating bulk entrainment with unaggregated and aggregated convection. *Geophys. Res. Lett.*, **45 (1)**, 455–462, https://doi.org/10.1002/2017gl076640.

Chou, M. D., W. L. Ridgway, and M. M. H. Yan, 1993: One-parameter scaling and exponential-sum fitting for water vapor and CO_2 infrared transmission functions. *J. Atmos. Sci.*, **50 (14)**, 2294–2303.

Delworth, T. L., and Coauthors, 2006: GFDL's CM2 global coupled climate models. part I: Formulation and simulation characteristics. *J. Climate*, **19 (5)**, 643–674, https://doi.org/10.1175/jcli3629.1.

Folkins, I., 2002: Origin of lapse rate changes in the upper tropical troposphere. *J. Atmos. Sci.*, **59 (5)**, 992–1005.

Folkins, I., M. Loewenstein, J. Podolske, S. J. Oltmans, and M. Proffitt, 1999: A barrier to vertical mixing at 14 km in the tropics: Evidence from ozonesondes and aircraft measurements. *J. Geophys. Res. Atmos.*, **104**, 22 095 –22 102.

Harries, J. E., 1997: Atmospheric radiation and atmospheric humidity. *Quart. J. Royal Meteorol. Soc.*, **123 (544)**, 2173–86.

Hartmann, D. L., and K. Larson, 2002: An important constraint on tropical cloud-climate feedback. *Geophys. Res. Lett.*, **29 (20)**, 1951–1954, https://doi.org/10.1029/2002GL015835.

Iacono, M. J., E. J. Mlawer, S. A. Clough, and J.-J. Morcrette, 2000: Impact of an improved longwave radiation model, RRTM, on the energy budget and thermodynamic properties of the NCAR community climate model, CCM3. *J. Geophys. Res.: Atmos.*, **105 (D11)**, 14 873–14 890, https://doi.org/10.1029/2000JD900091.

Jeevanjee, N., and S. Fueglistaler, 2020a: On the cooling-to-space approximation. *Journal of the Atmospheric Sciences*, **77 (2)**, 465–478, https://doi.org/10.1175/JAS-D-18-0352.1, publisher: American Meteorological Society.

Jeevanjee, N., and S. Fueglistaler, 2020b: Simple spectral models for atmospheric radiative cooling. *J. Atmos. Sci.*, **77 (2)**, 479–497, https://doi.org/10.1175/jas-d-18-0347.1.

Jeevanjee, N., and D. M. Romps, 2018: Mean precipitation change from a deepening troposphere. *Proc. Nat. Acad. Sci.*, **115 (45)**, 11 465–11 470, https://doi.org/10.1073/pnas.1720683115.

Khairoutdinov, M. F., and D. A. Randall, 2003: Cloud Resolving Modeling of the ARM Summer 1997 IOP: Model Formulation, Results, Uncertainties, and Sensitivities. *J. Atmos. Sci.*, **60 (4)**, 607–625, https://doi.org/10.1175/1520-0469(2003)060<0607:CRMOTA>2.0.CO;2.

Knutson, T. R., and S. Manabe, 1995: Time-Mean Response over the Tropical Pacific to Increased C02 in a Coupled Ocean-Atmosphere Model. *J. Climate*, **8 (9)**, 2181–2199, https://doi.org/10.1175/1520-0442(1995)008<2181:TMROTT>2.0.CO;2.

Accepted for publication in *Journal of Climate*. DOI 10.1175/JCLI-D-21-0861.1.

Koll, D. D. B., and T. W. Cronin, 2018: Earth's outgoing longwave radiation linear due to H_2O greenhouse effect. *Proc. Nat. Acad. Sci. U. S. A.*, **115 (41)**, 10 293–10 298, https://doi.org/10.1073/pnas.1809868115.

Liou, K. N., 2002: *An Introduction to Atmospheric Radiation*. 2nd ed., Academic Press, 583 pp.

Manabe, S., and R. T. Wetherald, 1967: Thermal Equilibrium of the Atmosphere with a Given Distribution of Relative Humidity. *J. Atmos. Sci.*, **24 (3)**, 241–259, https://doi.org/10.1175/1520-0469(1967)024<0241:TEOTAW>2.0.CO;2.

McFarlane, S. A., J. H. Mather, and T. P. Ackerman, 2007: Analysis of tropical radiative heating profiles: A comparison of models and observations. *J. Geophys. Res. Atmos.*, **112 (D14)**, https://doi.org/https://doi.org/10.1029/2006JD008290.

Mlawer, E. J., V. H. Payne, J.-L. Moncet, J. S. Delamere, M. J. Alvarado, and D. C. Tobin, 2012: Development and recent evaluation of the MT-CKD model of continuum absorption. *Phil. Trans. Royal Soc. A*, **370 (1968)**, 2520–2556, https://doi.org/doi:10.1098/rsta.2011.0295.

Mlawer, E. J., S. J. Taubman, P. D. Brown, M. J. Iacono, and S. A. Clough, 1997: Radiative transfer for inhomogeneous atmospheres: RRTM, a validated correlated-k model for the longwave. *J. Geophys. Res.: Atmos.*, **102 (D14)**, 16 663–16 682, https://doi.org/10.1029/97JD00237.

Morrison, H., and J. A. Milbrandt, 2015: Parameterization of cloud microphysics based on the prediction of bulk ice particle properties. Part I: Scheme description and idealized tests. *J. Atmos. Sci.*, **72 (1)**, 287–311, https://doi.org/10.1175/JAS-D-14-0065.1.

Petty, G., 2006: *A First Course in Atmospheric Radiation*. Sundog Publishing, Madison, Wisconsin.

Rodgers, C., and C. Walshaw, 1966: The computation of infrared cooling rate in planetary atmospheres. *Quart. J. Roy. Meteor. Soc.*, **92**, 67–92.

Romps, D. M., 2014a: An Analytical Model for Tropical Relative Humidity. *J. Climate*, **27 (19)**, 7432–7449, https://doi.org/10.1175/JCLI-D-14-00255.1.

Romps, D. M., 2014b: An analytical model for tropical relative humidity. *J. Climate*, **27 (19)**, 7432–7449.

Accepted for publication in *Journal of Climate*. DOI 10.1175/JCLI-D-21-0861.1.

Salathe, J., E. P., and D. L. Hartmann, 2000: Subsidence and upper-tropospheric drying along trajectories in a general circulation model. *J. Climate*, **13 (1)**, 257–63.

Singh, M. S., and P. A. O'Gorman, 2013: Influence of entrainment on the thermal stratification in simulations of radiative-convective equilibrium. *Geophys. Res. Lett.*, **40 (16)**, 4398–4403, https://doi.org/doi:10.1002/grl.50796.

Soden, B. J., and F. P. Bretherton, 1994: Evaluation of water-vapor distribution in general-circulation models using satellite-observations. *J. Geophys. Res.-Atmos.*, **99 (D1)**, 1187–1210.

Soden, B. J., R. T. Wetherald, G. L. Stenchikov, and A. Robock, 2002: Global cooling after the eruption of mount pinatubo: A test of climate feedback by water vapor. *Science*, **296**, 727–730.

Sokol, A. B., and D. Hartmann, 2022: Radiative cooling, latent heating, and cloud ice in the tropical upper troposphere. *J. Climate*, https://doi.org/10.1175/JCLI-D-21-0444.1.

Wing, A. A., and Coauthors, 2020: Clouds and convective self-aggregation in a multimodel ensemble of radiative-convective equilibrium simulations. *J. Adv. Model. Earth Syst.*, **12 (9)**, e2020MS002 138, https://doi.org/10.1029/2020MS002138.

Yamaguchi, T., D. A. Randall, and M. F. Khairoutdinov, 2011: Cloud Modeling Tests of the ULTIMATE–MACHO Scalar Advection Scheme. *Mon. Wea. Rev.*, **139 (10)**, 3248–3264, https://doi.org/10.1175/MWR-D-10-05044.1.

Zhou, W. Y., and S. P. Xie, 2019: A conceptual spectral plume model for understanding tropical temperature profile and convective updraft velocities. *J. Atmos. Sci.*, **76 (9)**, 2801–2814, https://doi.org/10.1175/jas-d-18-0330.1.

Accepted for publication in *Journal of Climate*. DOI 10.1175/JCLI-D-21-0861.1.